Liquid crystal dynamics in a photonic crystal cavity created by selective microfluidic infiltration

Liquid crystal dynamics in a photonic crystal cavity created by selective microfluidic infiltration

A. Casas Bedoya,[1,*] S. Mahmoodian,[1] C. Monat,[1] S. Tomljenovic-Hanic,[2] C. Grillet,[1] P. Domachuk,[1] E.C. Mägi,[1] B. J. Eggleton,[1] and R. W. van der Heijden[1,3]

[1]Centre for Ultrahigh bandwidth Devices for Optical Systems (CUDOS), Institute of Photonics and Optical Science (IPOS), School of Physics, University of Sydney, New South Wales 2006, Australia
[2]School of Physics, University of Melbourne, Parkville, VIC 3010, Australia
[3]COBRA Research Institute and Department of Applied Physics, Eindhoven University of Technology, PO Box 513, NL-5600MB Eindhoven, The Netherlands
**casas@physics.usyd.edu.au*

Abstract: A microfluidic double heterostructure cavity is created in a silicon planar photonic crystal waveguide by selective infiltration of a liquid crystal. The spectral evolution of the cavity resonances probed by evanescent coupling reveals that the liquid crystal evaporates, even at room temperature, despite its relatively low vapor pressure of 5×10^{-3} Pa. We explore the infiltration and evaporation dynamics of the liquid crystal within the cavity using a Fabry-Perot model that accounts for the joint effects of liquid volume reduction and cavity length variation due to liquid evaporation. While discussing how the pattern of the infiltrated liquid can be optimized to restrict evaporation, we find that the experimental behavior is consistent with basic microfluidic relations considering the small volumes of liquids and large surface areas present in our structure.

OCIS codes: (230.5298) Photonic crystals; (230.3720) Liquid-crystal devices; (130.5296) Photonic crystal waveguides.

References and links

1. C. Monat, P. Domachuk, and B. J. Eggleton, "Integrated optofluidics: A new river of light," Nat. Photonics **1**(2), 106–114 (2007).
2. D. Psaltis, S. R. Quake, and C. H. Yang, "Developing optofluidic technology through the fusion of microfluidics and optics," Nature **442**(7101), 381–386 (2006).
3. C. L. C. Smith, U. Bog, S. Tomljenovic-Hanic, M. W. Lee, D. K. C. Wu, L. O'Faolain, C. Monat, C. Grillet, T. F. Krauss, C. Karnutsch, R. C. McPhedran, and B. J. Eggleton, "Reconfigurable microfluidic photonic crystal slab cavities," Opt. Express **16**(20), 15887–15896 (2008).
4. M. Ebnali-Heidari, C. Grillet, C. Monat, and B. J. Eggleton, "Dispersion engineering of slow light photonic crystal waveguides using microfluidic infiltration," Opt. Express **17**(3), 1628–1635 (2009).
5. H. Kurt, and D. S. Citrin, "Reconfigurable multimode photonic-crystal waveguides," Opt. Express **16**(16), 11995–12001 (2008).
6. S. Tomljenovic-Hanic, C. M. de Sterke, and M. J. Steel, "Design of high-Q cavities in photonic crystal slab heterostructures by air-holes infiltration," Opt. Express **14**(25), 12451–12456 (2006).
7. F. Intonti, S. Vignolini, V. Türck, M. Colocci, P. Bettotti, L. Pavesi, S. L. Schweizer, R. Wehrspohn, and D. Wiersma, "Rewritable photonic circuits," Appl. Phys. Lett. **89**(21), 211117 (2006).
8. P. El-Kallassi, S. Balog, R. Houdré, L. Balet, L. Li, M. Francardi, A. Gerardino, A. Fiore, R. Ferrini, and L. Zuppiroli, "Local infiltration of planar photonic crystals with UV-curable polymers," J. Opt. Soc. Am. B **25**(10), 1562 (2008).
9. D. Erickson, T. Rockwood, T. Emery, A. Scherer, and D. Psaltis, "Nanofluidic tuning of photonic crystal circuits," Opt. Lett. **31**(1), 59–61 (2006).
10. S. H. Kim, J. H. Choi, S. K. Lee, S. H. Kim, S. M. Yang, Y. H. Lee, C. Seassal, P. Regrency, and P. Viktorovitch, "Optofluidic integration of a photonic crystal nanolaser," Opt. Express **16**(9), 6515–6527 (2008).
11. H. H. J. E. Kicken, P. F. A. Alkemade, R. W. van der Heijden, F. Karouta, R. Nötzel, E. van der Drift, and H. W. M. Salemink, "Wavelength tuning of planar photonic crystals by local processing of individual holes," Opt. Express **17**(24), 22005–22011 (2009).

#136250 - $15.00 USD Received 7 Oct 2010; revised 7 Nov 2010; accepted 6 Dec 2010; published 10 Dec 2010

12. C. L. C. Smith, D. K. C. Wu, M. W. Lee, C. Monat, S. Tomljenovic-Hanic, C. Grillet, B. J. Eggleton, D. Freeman, Y. Ruan, S. Madden, B. Luther-Davies, H. Giessen, and Y.-H. Lee, "Microfluidic photonic crystal double heterostructures," Appl. Phys. Lett. **91**(12), 121103 (2007).
13. U. Bog, C. L. C. Smith, M. W. Lee, S. Tomljenovic-Hanic, C. Grillet, C. Monat, L. O'Faolain, C. Karnutsch, T. F. Krauss, R. C. McPhedran, and B. J. Eggleton, "High-Q microfluidic cavities in silicon-based two-dimensional photonic crystal structures," Opt. Lett. **33**(19), 2206–2208 (2008).
14. C. Karnutsch, C. L. C. Smith, A. Graham, S. Tomljenovic-Hanic, R. McPhedran, B. J. Eggleton, L. O'Faolain, T. F. Krauss, S. Xiao, and N. A. Mortensen, "Temperature stabilization of optofluidic photonic crystal cavities," Appl. Phys. Lett. **94**(23), 231114 (2009).
15. K. Busch, and S. John, "Liquid-Crystal Photonic-Band-Gap materials: the tunable electromagnetic vacuum," Phys. Rev. Lett. **83**(5), 967–970 (1999).
16. S. W. Leonard, J. P. Mondia, H. M. van Driel, O. Toader, S. John, K. Busch, A. Birner, U. Gösele, and V. Lehmann, "Tunable two-dimensional photonic crystals using liquid-crystal infiltration," Phys. Rev. B **61**(4), R2389–R2392 (2000).
17. G. Mertens, T. Röder, H. Matthias, H. Marsmann, H. S. R. Kitzerow, S. L. Schweizer, C. Jamois, R. B. Wehrspohn, and M. Neubert, "Two and three-dimensional photonic crystals made of macroporous silicon and liquid crystals," Appl. Phys. Lett. **83**(15), 3036 (2003).
18. S. M. Weiss, H. Ouyang, J. Zhang, and P. M. Fauchet, "Electrical and thermal modulation of silicon photonic bandgap microcavities containing liquid crystals," Opt. Express **13**(4), 1090–1097 (2005).
19. Y. Shimoda, M. Ozaki, and K. Yoshino, "Electric field tuning of a stop band in a reflection spectrum of synthetic opal infiltrated with nematic liquid crystal," Appl. Phys. Lett. **79**(22), 3627 (2001).
20. Ch. Schuller, F. Klopf, J. P. Reithmaier, M. Kamp, and A. Forchel, "Tunable photonic crystals fabricated in III-V semiconductor slab waveguides using infiltrated liquid crystals," Appl. Phys. Lett. **82**(17), 2767 (2003).
21. R. Ferrini, J. Martz, L. Zuppiroli, B. Wild, V. Zabelin, L. A. Dunbar, R. Houdré, M. Mulot, and S. Anand, "Planar photonic crystals infiltrated with liquid crystals: optical characterization of molecule orientation," Opt. Lett. **31**(9), 1238 (2006).
22. B. Maune, M. Loncar, J. Witzens, M. Hochberg, T. Baehr-Jones, D. Psaltis, A. Scherer, and Y. Qiu, "Liquid-crystal electric tuning of a photonic crystal laser," Appl. Phys. Lett. **85**(3), 360 (2004).
23. B. Maune, J. Witzens, T. Baehr-Jones, M. Kolodrubetz, H. Atwater, A. Scherer, R. Hagen, and Y. Qiu, "Optically triggered Q-switched photonic crystal laser," Opt. Express **13**(12), 4699–4707 (2005).
24. P. El-Kallassi, R. Ferrini, L. Zuppiroli, N. Le Thomas, R. Houdré, A. Berrier, S. Anand, and A. Talneau, "Optical tuning of planar photonic crystals infiltrated with organic molecules," J. Opt. Soc. Am. B **24**(9), 2165 (2007).
25. Ch. Schuller, J. P. Reithmaier, J. Zimmermann, M. Kamp, A. Forchel, and S. Anand, "Polarization-dependent optical properties of planar photonic crystals infiltrated with liquid crystal," Appl. Phys. Lett. **87**(12), 121105 (2005).
26. J. Martz, R. Ferrini, F. Nüesch, L. Zuppiroli, B. Wild, L. A. Dunbar, R. Houdré, M. Mulot, and S. Anand, "Liquid crystal infiltration of InP-based planar photonic crystals," J. Appl. Phys. **99**(10), 103105 (2006).
27. M. A. Dündar, H. H. J. E. Kicken, A. Yu. Silov, R. Nötzel, F. Karouta, H. W. M. Salemink, and R. W. van der Heijden, "Birefringence-induced mode-dependent tuning of liquid crystal infiltrated InGaAsP photonic crystal nanocavities," Appl. Phys. Lett. **95**(18), 181111 (2009).
28. M. W. Lee, C. Grillet, C. G. Poulton, C. Monat, C. L. Smith, E. Mägi, D. Freeman, S. Madden, B. Luther-Davies, and B. J. Eggleton, "Characterizing photonic crystal waveguides with an expanded k-space evanescent coupling technique," Opt. Express **16**(18), 13800–13808 (2008).
29. P. Etchegoin, A. Fainstein, and R. G. Pregliasco, "Optical nonlinearities in the supercooled phase of nematic liquid crystal drops," Physica D **134**(1), 144–151 (1999).
30. S. Brugioni, and R. Meucci, "Refractive indices of liquid crystals E7 and K15 in the mid- and near-IR regions," J. Opt. Technol. **73**, 315 (2006).
31. C. Grillet, D. Freeman, B. Luther-Davies, S. Madden, R. McPhedran, D. J. Moss, M. J. Steel, and B. J. Eggleton, "Characterization and modeling of Fano resonances in chalcogenide photonic crystal membranes," Opt. Express **14**(1), 369–376 (2006).
32. M. Elbaum, and S. G. Lipson, "How does a thin wetted film dry up?" Phys. Rev. Lett. **72**(22), 3562–3565 (1994).
33. Data provided by supplier, Nematel GmbH, Mainz, Germany.
34. Y. Tanaka, T. Asano, and S. Noda, "Design of Photonic Crystal Nanocavity With Q-Factor of ~10^9," J. Lightwave Technol. **26**(11), 1532–1539 (2008).
35. S. Karnutsch, Tomljenovic-Hanic, C. Monat and B. J. Eggleton "Reconfigurable photonic crystal circuits using microfluidics," *in Optofluidics*, Y. Fainman, L. Lee, D. Psaltis, and C. Yang, Eds, (McGraw-Hill, New York, NY., 2009)
36. I. Langmuir, "The Vapor Pressure of Metallic Tungsten," Phys. Rev. **2**(5), 329–342 (1913).
37. F. Intonti, S. Vignolini, F. Riboli, M. Zani, D. S. Wiersma, L. Balet, L. H. Li, M. Francardi, A. Gerardino, A. Fiore, and M. Gurioli, "Tuning of photonic crystal cavities by controlled removal of locally infiltrated water," Appl. Phys. Lett. **95**(17), 173112 (2009).
38. L. R. Fisher, R. A. Gamble, and J. Middlehurst, "The Kelvin equation and the capillary condensation of water," Nature **290**(5807), 575–576 (1981).
39. C. A. Barrios, M. Holgado, O. Guarneros, K. B. Gylfason, B. Sánchez, R. Casquel, and H. Sohlström, "Reconfiguration of microring resonators by liquid adhesion," Appl. Phys. Lett. **93**(20), 203114 (2008).

#136250 - $15.00 USD Received 7 Oct 2010; revised 7 Nov 2010; accepted 6 Dec 2010; published 10 Dec 2010

1. Introduction

The inherently mobile fluid phase is naturally suited for dynamic infiltration or withdrawal in nm or micron scale photonic structures [1]. This flourishing field of optofluidics [1,2], the combination of microfluidics and photonics, has been successfully applied to tuning the optical properties of photonic crystal (PhC) devices [3]. PhCs are naturally suited for optofluidic tuning due to their Sub-wavelength scale voids that can house fluids. Infiltrating only a pre-selected set of holes of the PhC microstructure enables finer control over the PhC optical properties when compared to coarser infiltration [4]. Selective PhC infiltration also provides an elegant approach for fabricating arbitrary PhC defect structures without the need for lithography, such as waveguides [5] and cavities [6].

The optical performance of the infiltrated PhC depends somewhat upon the quality and control of the infiltration process. One infiltration method using a computer controlled micropipette actuated in three dimensions [7] enables nearly single hole resolution. Other local infiltration methods rely on local photo-polymerization of a liquid monomer [8], nanofluidic circuits bonded onto the PhC chip [9,10], or lithographic masking [11]. Recently, an approach for creating high Q double heterostructure PhC cavities by selectively infiltrating a PhC waveguide with liquids was proposed [6] and demonstrated in chalcogenide glass [12] and Si membranes [3,13]. These cavities relied on the infiltration of immersion oil, whose thermal properties were subsequently exploited to induce a temperature-insensitive cavity [14].

An attractive aspect of optofluidic tuning is the wide range of optical properties (some not even available in solids) available through fluid chemistry. A good example are liquid crystals (LCs), whose refractive index can be tuned with temperature, electric or optical fields, over a far greater range than solid materials [15]. This unique property has been leveraged in several demonstrations of tunable PhC devices based on LC infiltration in two-dimensional macroporous Si [16–18], and three-dimensional inverse opals [19]. Tuning of planar PhC devices through controlling the orientation of the LCs with temperature gradients [20,21], with electrical [22] or optical [23,24] fields has also been reported. The anisotropic optical properties of LCs were revealed by observing their behavior under different light polarizations [25–27]. However, most of these demonstrations were performed by fully immersing the PhC structures in LC solutions, involving relatively large volumes of LCs in the final devices in an essentially non-integrated way.

In this work, we report the first PhC cavities created by selective LC infiltration. These double heterostructure cavities are obtained by infiltrating an ~10μm wide section of a silicon PhC waveguide and the associated resonances have a measured Q-factor in excess of 10000. We investigate the dynamics of the LC in our structure, both at 20°C temperature and above the phase transition temperature, and explore its stability due to liquid transport and evaporation. We analyze our optical data by introducing a Fabry-Perot model that accounts for the joint effects of liquid volume reduction and cavity length variation due to liquid evaporation. Our results demonstrate that the LC evaporates, even at 20°C temperature, despite its relatively low vapor pressure (5×10^{-3} Pa) and that even modest evaporation rates (10% liquid volume reduction in ~35min) greatly affect the spectral signature of our cavity. Evaporation is found to be consistent with the microfluidic equations at the relevant length scales of our system, and its significant impact is due to the small volumes (~0.19 attoliters) of liquids involved in our structure. We offer a solution to this issue through managing liquid reservoirs in the surrounding of the cavity to reduce the evaporation rate.

2. Sample and experimental methods

Figure 1(a) shows an optical microscope image of the silicon PhC waveguide. It is created as a Si membrane by lithographic methods and is suspended in air after the final underetching of the Silicon On Insulator (SOI) structure using HF solution. The PhC waveguide is obtained by omitting one row of holes along ΓK and shifting the two adjacent PhC regions slightly, so that the distance between the holes close to the linear defect is 0.9 times their distance in the lattice

#136250 - $15.00 USD Received 7 Oct 2010; revised 7 Nov 2010; accepted 6 Dec 2010; published 10 Dec 2010

("W0.9 waveguide"). The lattice period a is 410nm, the membrane thickness 220 nm, the hole radius r is $(0.33 \pm 0.06)a$ and the total length of the waveguide is 25μm.

The dispersion relation of the W0.9 waveguide calculated using a commercial 3D plane wave expansion method solver for periodic optical structures, is plotted in Fig. 1(b) for (*i*) the initial waveguide with air holes ("Uninfiltrated PhC") and (*ii*) assuming a dielectric with refractive index $n = 1.54$ (i.e. close to the LC index) in all holes ("infiltrated PhC"). A Si refractive index of 3.52 is used and the r/a ratio is fitted to 0.334 from the experimental value of the fundamental mode cut-off that is measured to be around $a/\lambda = 0.287$ (cut-off frequency). Also shown in Fig. 1(b) is the PhC lower band edge, and the light line of the air surrounding the membrane. Note that in the following, we assume that our infiltrated PhC structure consists of certain amount of liquid in the holes (see section 4) with a thin top layer of liquid above the membrane. First, the contact angle of a drop of this liquid onto the sample surface shows that this kind of liquid has wetting properties that allows for the holes to be (at least partially) infiltrated. Secondly, the large frequency shift of the dispersion that is inferred from the experimental results of section 3 cannot be accounted for by the sole presence of a top layer, as its effect on the dispersion is much less than the filling of the holes (see section 4).

The selective infiltration of the W0.9 PhC waveguide was monitored under a 50X magnification objective (see (3) for further details). A 0.5 ± 0.2μm inner diameter micropipette, filled with the LC, was brought in contact with the sample and moved along its surface with a 50nm spatial resolution micromanipulator, to "write" the infiltrated region with the desired dimensions. The holes in contact with the pipette filled through capillary action, resulting in a liquid volume inside the holes held against gravity by surface tension. Figure 1(a) displays the resulting strip of width 9 ± 1μm associated with the infiltrated region encompassed between two uninfiltrated regions of the W0.9 waveguide. The PhC structure was probed by analyzing the transmission through a looped, tapered telecommunication single mode silica fiber, evanescently coupled to the waveguide [28]. For the experiments reported here, the fiber was always kept in contact with the PhC waveguide [12]. The dispersion curve of the taper, with diameter of 1.0 ± 0.5 μm and radius of curvature 10.0 ± 0.5μm, is plotted in Fig. 1(b). The coupling efficiency is maximum where the dispersion curves of the tapered fiber and the waveguide mode intersect; however, the use of a highly curved taper allows coupling over a broader range of wavevectors around this point [28]. The emission from four Light Emitting Diodes with a bandwidth between 1250 and 1650nm was used as a broadband source and the spectrum of the light transmitted through the taper after interaction with the PhC was measured with an Optical Spectrum Analyzer using 0.06nm resolution and spanning across 1410-1460nm .

The LC 4-pentyl-4'-cyanobiphenyl (known as K15 or 5CB) was used for the infiltration. It has a solid - nematic liquid transition at 23 °C, but in practice remains in a supercooled liquid nematic state at temperatures well below 20 °C [29]. It has a nematic – isotropic liquid transition at the clearance temperature $T_c = 35$ °C. The ordinary and extraordinary refractive indices of the nematic state at infrared wavelengths near 1.55 μm are $n_o = 1.50$ and $n_e = 1.67$, respectively, while the isotropic refractive index above T_c is $n_{iso} = 1.54$ [30].

The infiltration is carried out at 20°C temperature, well above the melting temperature, but below T_c. For the second part of the measurements, the infiltrated PhC sample is mounted on a Peltier module to vary the temperature from 20 to 55 °C.

#136250 - $15.00 USD Received 7 Oct 2010; revised 7 Nov 2010; accepted 6 Dec 2010; published 10 Dec 2010

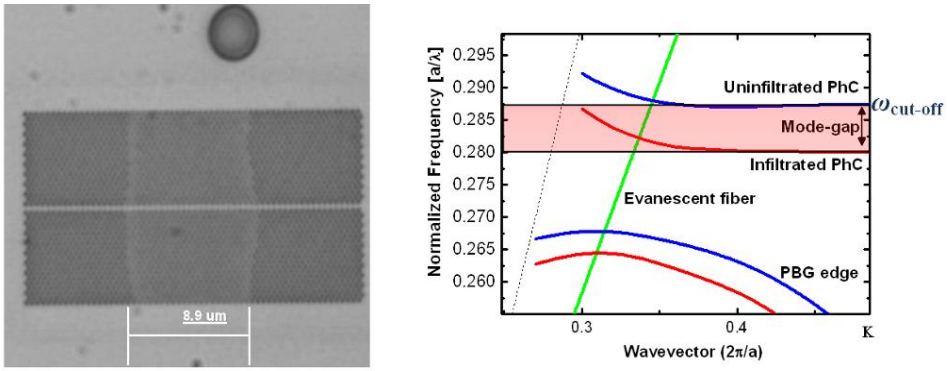

Fig. 1. (a) Optical microscope image of infiltrated cavity. (b) Calculated dispersion relations of the W0.9 waveguide without infill ("Uninfiltrated PhC"), and after infiltration ("infiltrated PhC").

3. Experimental results

3.1 Liquid crystal induced cavities

A reference spectrum of the waveguide probed before infiltration is shown in Fig. 2(a) ("before"). Around the normalized frequency $a/\lambda = 0.288$, light from the taper is coupled to the waveguide, resulting in a dip in the fiber transmission. The $a/\lambda = 0.287$ frequency corresponds to the cut-off frequency of the uninfiltrated waveguide. The fine spectral structure that is superimposed onto the main transmission dip is due to the reflections at the waveguide ends.

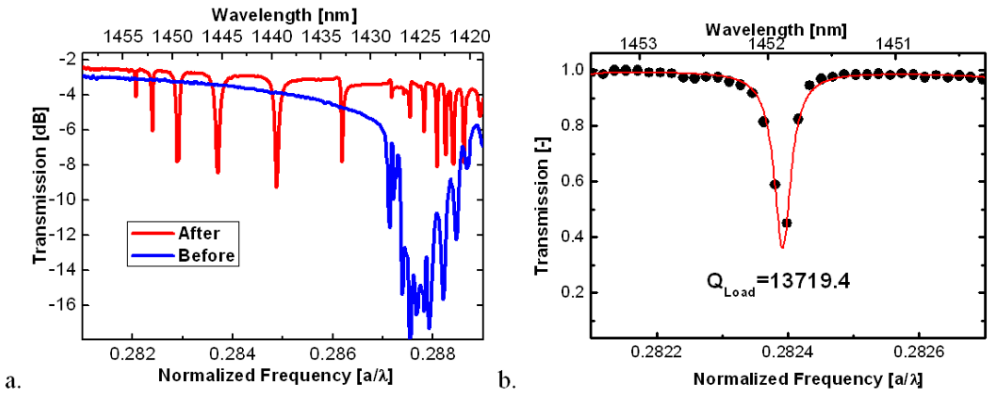

Fig. 2. (a) Transmission spectrum through the tapered fiber coupled to the waveguide before and after infiltration. (b) Close up of one resonance along with a Lorentzian fit to extract the (loaded) Q-factor.

After the waveguide is infiltrated with the LC over a 10 ± 1μm long section, the red spectrum of Fig. 2(a) is measured at 20°C. The additional series of dips appearing at longer wavelengths corresponds to resonances of the double heterostructure cavity, i.e. bound within the infiltrated section and reflected at the interfaces with the uninfiltrated regions. These reflections are more pronounced when the dispersion curve of the infiltrated section has no overlap with the dispersion curve of the uninfiltrated section, in the so called mode-gap. Note, however, that the spectrum is also modified by the infiltration where the two dispersion curves overlap, above 0.287 [31]. Figure 2(b) shows a close-up of one resonance in the mode gap. A conservative value for the quality factor $Q \sim 10^4$ can be inferred [13], which is limited by the spectrometer resolution, and decreased by the coupling with the fiber. The free spectral range

#136250 - $15.00 USD Received 7 Oct 2010; revised 7 Nov 2010; accepted 6 Dec 2010; published 10 Dec 2010

of the cavity resonances decreases towards shorter frequencies, as expected from the infiltrated waveguide dispersion that flattens out near 0.280 according to the bandstructure shown in Fig. 1(b) [3,28].

An a priori unexpected phenomenon, not observed in the previous PhC infiltration at 20°C [3,12], is shown in Fig. 3(a) for a LC infiltrated cavity roughly similar to that of Fig. 1(a). All resonances are observed to shift to larger frequencies with time and closer to the uninfiltrated waveguide mode, while new spectral dips appear at short frequencies. These shifts may be attributed to evaporation of the liquid, which results in both a shorter cavity length and to less liquid inside the holes.

A confirmation of the LC evaporation was obtained from the spectral signature of the cavity when the sample was subsequently heated, as shown in Fig. 3(b). The top-most spectrum, 35 min after infiltration, corresponds to the 20°C reference, and is the bottom spectrum in Fig. 3(a). At 37 min, the heater was turned on, which brought the sample in less than 10 seconds to a constant temperature of 55 ± 3°C, well above the T_c of the LC. The LC phase transition was monitored by visual observation of the clearance of a LC droplet added on the Si chip, away from the PhC. At high temperature, the spectral dips in the transmission are observed to shift much faster than at 20 °C, which is related to the higher evaporation rate.

A quick assessment of the behavior of the LC infiltrated PhC is generally done by measuring the thermal dependence near T_c rather than by applying strong electric or optical fields [16,17,20,21,27]. Considering a maximum LC refractive index change Δn of ~-0.05 (n_{iso} minus some average of n_o and n_e), and an estimated sensitivity $\Delta\lambda/\Delta n$ = 60 nm/RIU (Refractive Index Unit) for this type of cavity resonances [13], we only expect a few nanometer wavelength shift, most likely towards shorter wavelengths, due to the LC phase transition near T_c. However, at t = 37 min, before evaporation strikes in, we observe a slight increase (~1nm) of the resonance wavelengths. This is due to the combination of the thermo-optic effect in Si, which should shift the resonances by ~3nm towards longer wavelengths [14], and the LC refractive index change that has the opposite effect. The signature associated with the LC phase transition is therefore partly hidden in this experiment by LC evaporation and the Si thermo-optic properties.

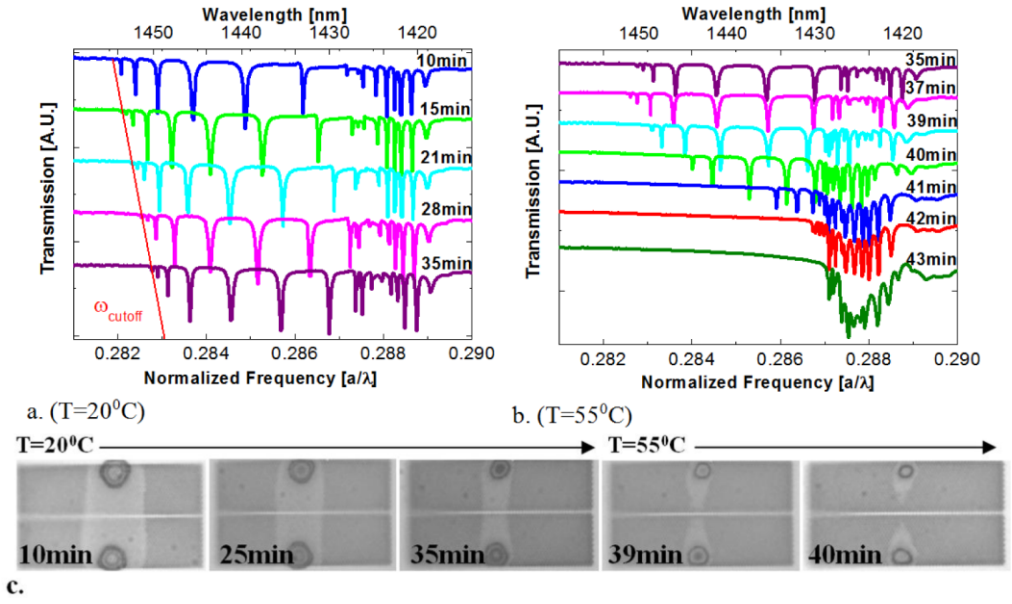

Fig. 3. (a) Transmission spectra through the tapered fiber coupled to the waveguide at different times after the infiltration at 20 °C. (b) Same as (a), but at a higher temperature (55 °C) after the heater is turned on at 37 min. (c) Optical microscope images showing the time evolution of a LC infiltrated cavity at the two different temperatures investigated.

#136250 - $15.00 USD Received 7 Oct 2010; revised 7 Nov 2010; accepted 6 Dec 2010; published 10 Dec 2010

3.2 Evaporation of the liquid crystal

We further investigate the dynamics of LC evaporation at room temperature by monitoring an infiltrated PhC structure over time under a microscope. A PhC area uniformly infiltrated with LC as in Fig. 1(a) fully disappears within around 40 minutes after infiltration. During this process, we observed that the LC evaporation in the center of the infiltrated region was, at least partially, compensated by liquid transport from the boundaries of the layer towards the center. A similar effect has been reported for large areas of thin films, which do not evaporate uniformly [32]. This provides a clue for stabilizing the PhC infiltrated section. We repeat the infiltration but leave two large droplets on both sides of the infiltrated PhC area that may serve as a reservoir to compensate for evaporation (Fig. 3(c)). This approach works relatively well: at RT, the liquid strip lasts three times longer (~120min) than without the drops, and only disappears after the drops themselves have evaporated. Liquid transport across the infiltrated section can thus improve the stability of the infiltrated area, and the lifetime of liquid strips can be controlled by designing the geometry to accommodate sufficiently large liquid reservoirs in contact with the strip.

The data associated with Fig. 3(a,b) were measured for an infiltrated PhC cavity including similar droplets to that shown on Fig. 3(c). The optical measurements can be thus directly correlated with the physical change of the cavity due to LC evaporation, as monitored on Fig. 3(c), at 20°C and 55°C. The length of the infiltrated region is seen to steadily decrease with time (up to 35min), indicating that film transport from the drops is not sufficient to fully compensate for the liquid evaporation near the boundaries. This may be partly due to the size of the droplets that were narrower than the initial cavity length in this case. In addition, the surface transport is likely limited by the liquid's viscosity, which is rather high for the LC K15, 2.4×10^{-5} m^2/s at 20 °C, i.e. 24 times larger than that for water [33]. While the spectral evolution reflects the joint effects of liquid volume reduction and cavity length shrinkage due to liquid evaporation, the waveguide frequency cut-off primarily gives an estimation of the volume of liquid in the holes (and possibly on top of them). The observation on Fig. 3(c) that the contrast of the infiltrated PhC does not change dramatically over the first 35 min duration is consistent with the slight liquid volume reduction (~10%) inferred from the analysis of the cut-off frequency in the next section.

Turning on the heater at 37 min accelerates the evaporation rate, as attested by both optical measurements and the images of Fig. 3(c). After few min, a contrast change is observed near the center between the drops, suggesting that the film starts to quickly evaporate from the center as well. The fast reduction of liquid volume results in a rapid shrinkage of the mode gap and all resonances start to collapse close to the frequency cut-off of the uninfiltrated PhC waveguide, as observed in Fig. 3(b). At this high evaporation rate the liquid transport across the surface can no longer compensate for evaporation.

In previous works [8,20–27] the samples were immersed in the LC and then retracted, or a macroscopic drop of LC was put on the surface, so that the total amount of liquid was orders of magnitude higher than in the present case. The evaporation time is proportional to the volume-to-surface ratio, and therefore roughly scales with the linear dimension of the system, which is 2 to 3 orders of magnitude smaller for the present system than for the previous cases. The observation from Fig. 3(c) that the typical timescale for evaporation is ~1 hr, explains why evaporation was not noticeable in the previous experiments.

4. Analysis of the optical data: modeling the liquid crystal evaporation

The optical data of the LC infiltrated PhC are difficult to quantitatively analyze due to the joint effects of liquid volume reduction and cavity length shrinkage induced by liquid evaporation. In addition, the flattening of the waveguide dispersion near the cut-off frequency, and the use of the evanescent coupling restricts the number of resonant modes that could be probed to ~5-6 within the mode-gap. One consequence is that the approximation of the waveguide cut-off frequency with the lowest frequency measured resonance is inaccurate. We try in this section to obtain more quantitative information from the free spectral range and the

#136250 - $15.00 USD Received 7 Oct 2010; revised 7 Nov 2010; accepted 6 Dec 2010; published 10 Dec 2010

resonance frequencies measured at 20°C, by modeling the cavity as a conventional Fabry–Pérot (FP) interferometer, where the transmission *T* is given by:

$$T = \frac{1}{1 + F\,\mathrm{Sin}^2(kL)}. \quad (1)$$

In Eq. (1), F is the finesse coefficient and L is the effective cavity length, which may be different from the physical length of the infiltrated region, due to the evanescent field penetration at the heterostructure boundaries. From Eq. (1), the maximum transmission is obtained when the wavevectors k_m of the FP modes satisfy the condition $k_m L = m\pi$, with the integer (m) being the order of the cavity mode. Note that the fiber transmission experimentally probed is proportional to 1-*T*.

We fit the calculated dispersion presented in Fig. 1(b) with a function $\omega(k_{red})$ relating the reduced wavevector $k_{red} = k/(2\pi/a)$ and the reduced frequency $\omega = a/\lambda$ through:

$$\omega(k) = \omega_0 + 80\left(k_{red} - \frac{1}{2}\right)^6, \quad (2)$$

with ω_0 the cutoff frequency. The underlying assumption is that the liquid infiltration only affects the frequency position of the dispersion (through changing ω_0 in Eq. (2)) without changing its curvature. This approximation is validated by 3D bandstructure calculations that are fitted by Eq. (2) on Fig. 4(a) for both the uninfiltrated case and the infiltrated cases, with ω_0 values equal to 0.287 and 0.280, respectively. Note that ω_0 therefore contains all the information associated with the liquid infiltration, such as the amount of liquid inside the holes and the potential presence of a top layer of liquid [6], but it is completely independent on the cavity length. Figure 4(a) also shows the simulated dispersion curve when 74% of the hole volume is filled with liquid (brown solid line), as well as the results obtained in the presence of a top layer of liquid with (brown dashed line) or without (blue dashed line) LCs in the holes. These results show that the presence of a thin top layer (10-50nm) of liquid and its thickness variation has a restricted effect on the waveguide dispersion, and that the percentage of liquid inside the holes is the main factor responsible for the shift in the dispersion curve.

In order to correlate the experimental resonances, approximated by FP modes, with the volume of liquid within the PhC, we search for the value of ω_0 for which the dispersion given by Eq. (2) can accommodate the FP mode wavevectors $k_m(\omega_0) = k_m(\omega_0, \omega_m)$ with a wavector spacing Δk equal to π/L. This allows us to unambiguously relate the resonance frequencies ω_m measured for a particular time and amount of liquid with the associated waveguide dispersion $\omega(k)$ determined by ω_0. The wavevectors k_m are searched in the second Brillouin zone (between π/a and $2\pi/a$) since the back folding into the first Brillouin zone has no physical meaning in a conventional FP, where both the mode frequency and the wavector increase with the order of the mode.

We can therefore create a set of equations that allow us to find unique solutions for ω_0, m and L, by using three consecutive experimental resonances with wavevectors k_m, k_{m-1} and k_{m-2}:

$$\frac{m\pi}{k_m} = \frac{(m-1)\pi}{k_{m-1}} = \frac{(m-2)\pi}{k_{m-2}}. \quad (3)$$

The cut off frequency ω_0 obtained from our model using the data of Fig. 3(a) is plotted in Fig. 4(b) as a function of time (blue triangles). To estimate the associated liquid volume reduction, we include on Fig. 4(b) the waveguide cut-off frequency calculated using a plane wave method, versus the percentage of liquid into the PhC (solid lines), for a LC refractive index of 1.5, 1.6 and 1.66, respectively, due to the uncertainty on this value at 20°C ($1.50 < n_{LC} < 1.67$). Although the absolute amount of liquid depends on the LC index, we can infer from this plot that it is around 74% +/–8%, 20 minutes after the infiltration. In addition,

#136250 - $15.00 USD Received 7 Oct 2010; revised 7 Nov 2010; accepted 6 Dec 2010; published 10 Dec 2010

independently on the LC index value, the relative variation of ω_0 retrieved from the experiment can be correlated with a reduction of the liquid volume by ~10% (top axis). The roll-off of the ω_0 increase over time, which deviates from the calculated linear trends, suggests that the evaporation rate is slightly reduced; this is consistent with the LC strip behaviour observed when the infiltrated length reaches the diameter of the LC droplet reservoirs.

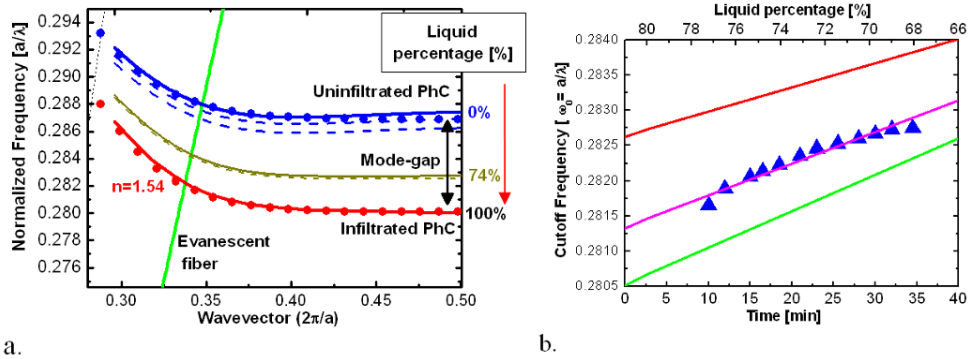

Fig. 4. (a) Calculated dispersion relations of the W0.9 waveguide before infiltration and after infiltration (lines), with LC index 1.54. (Blue and red dots) obtained using Eq. (2). (Dashed lines) correspond to dispersion for a 10nm and 50nm top layer only (blue) and 10nm top layer plus partially (74%) infiltrated PhC (brown) (b) (Blue triangles) Cut off frequency versus time (bottom axis), obtained from the FP model using three consequential FP resonance from the experimental data of Fig. 3 and cutoff frequencies calculated with Bandsolve for varying amount of liquid in the PhC (top axis) and three different values of the LC index of (red) 1.5, (purple) 1.6 and (green) 1.66.

Additionally, the model yields time evolution of the effective cavity length L, as plotted on Fig. 5. The inferred values decrease from 16 ± 1μm to 9.9μm. They are larger than the physical length of 10 ± 1μm measured for the initial infiltrated PhC. Since the modes of double heterostructure cavities are typically weakly bound along the direction of the photonic crystal waveguide, the effective length, especially of higher order modes, is larger than the physical length of the cavity [34,35]. Again the roll-off in the cavity size shrinkage observed in Fig. 5 agrees with our experimental observation that the LC drops were able to reduce the evaporation rates through liquid transport across the LC infiltrated section.

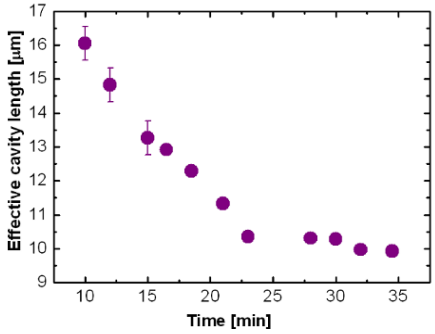

Fig. 5. . Calculated effective cavity length obtained from Eq. (3).

To confirm the validity of our FP model that only considers three experimental resonances from each spectrum, the modeling results (1-T) with ω_0 and L varying as per Figs. 4 and 5 are plotted on Fig. 6 along with the various spectra measured at 20 °C temperature. A relatively good agreement is obtained for most of the measured resonances. Some discrepancies can be noted, though, for some high frequency resonances, where the model tends to predict higher frequencies than the experiment. This again is the result of an increased penetration length [34,35] of the high frequency mode into the uninfiltrated waveguide, which is not taken into

#136250 - $15.00 USD Received 7 Oct 2010; revised 7 Nov 2010; accepted 6 Dec 2010; published 10 Dec 2010

account in our model, where the effective L is assumed to be the same for all modes at a given time.

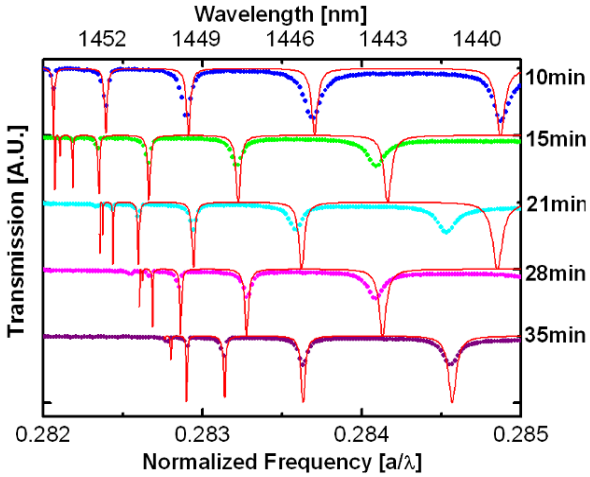

Fig. 6. Transmission spectra through the tapered fiber coupled to the waveguide at different times after the infiltration at 20 °C in the resonances region (color dots), and FP modes reconstruction using Eq. (1) for different times. (Red lines)

5. Discussion

At first sight, the rapid evaporation of the LC, even at 20°C temperature might be surprising as its vapor pressure is only 5×10^{-3} Pa (4×10^{-1} Pa at 100 °C) [33], in the range of typical low vapor pressure liquids like vacuum pump oils. It is also counterintuitive to the observation that macroscopic amounts of LC droplets, say 1 mm^3, do not noticeably dry over periods of months. While the evaporation rate is difficult to estimate, as it critically depends on the air flow conditions, an absolute upper limit can be obtained from the evaporation into vacuum, which is well defined and well approximated by the Langmuir equation [36]:

$$\frac{dm}{dt} = p_s \sqrt{\frac{M}{2\pi RT}}, \tag{4}$$

where dm/dt is the mass loss rate per unit area, p_s is the saturated vapor pressure, M the molecular weight (0.249 kg/Mol), R the ideal gas constant, and T the temperature. From the density of LC K15 (1.008×10^3 kg/m^3), one obtains a volume loss rate of 2×10^{-8} m^3/m^2s, or layer thickness decrease of 20 nm/s. This is three orders of magnitude faster than the observed evaporation rate, showing that the latter is reasonable. The decreasing of the cut off resonance frequency, in Fig. 3(a, b) is proportional to the evaporation rate, which in turn is proportional to the saturated vapor pressures. From the Clausius-Clapeyron relation, the vapor pressure may be estimated by interpolating the pressure values known at 20 and 100 °C. This yields a vapor pressure at 55 °C an order of magnitude higher than at 20 °C, in fair agreement with the striking changes in Fig. 3(b).

Vapor pressure, and so evaporation, is influenced by small geometries. An estimate of these effects can be made through the Kelvin equation, which relates the vapor pressure above a curved surface to the saturated vapor pressure. The Kelvin equation reads:

$$p = p_s \exp\left(\frac{-p_{cap} V_{mol}}{RT}\right), \tag{5}$$

where p is the vapor pressure above a curved surface with curvature radius r, $p_{cap} = 2\gamma/r$ is the capillary pressure where γ is the surface tension, and V_{mol} is the molar volume of the liquid.

#136250 - $15.00 USD Received 7 Oct 2010; revised 7 Nov 2010; accepted 6 Dec 2010; published 10 Dec 2010

With the reasonable assumption that γ is in the same range as for any liquid (~25 mN/m), taking the hole radius as a measure for r, the exponent is very close to 1. With the hole diameter to height ratio close to 1, flow impedance limitations will also be negligible. Consequently, geometry effects can be ignored.

Liquid vapor pressures occur in a very large range and there is an abundance of liquids with vapor pressures at room temperature many orders of magnitude lower than that of the LC used in this work (down to 10^{-8} Pa or less at room temperature). Evaporation of immersion oil from an infiltrated PhC cavity [3,12–14] was not observed over a period of several hours. This study points towards the necessity to use PhC structures infiltrated with moderate or high vapor pressure liquids in a sealed environment with a reservoir liquid to maintain a saturated vapor pressure. Alternatively, the use of a microfluidic circuit bonded onto the PhC may be preferred to continuously flush the LC in the targeted area of the PhC chip [8].

The dynamics and stability of small volumes of liquids in PhC structures is not straightforward and is far from being fully understood. Besides the work from our group, the earlier experiment on local infiltration of a PhC [7] used dyes dissolved in water without noticing any stability issues. Intonti et al. recently reported the infiltration with water of a single, 550 nm diameter, PhC hole with a total volume of 0.02 femtoliter, and it being stable for a period of weeks [37]. By laser-heating of the cavity to ~36 K, the water could be evaporated in about 20 hours. It is known from experiments that the vapor pressure of water in confined geometries has substantial deviations from the Kelvin equation [38], but these are not sufficient to explain the reported stability. However, water may represent a particular case, as it is present in the ambient atmosphere. Another remarkable report is the filling of 170 nm wide slots in slotted ring resonators of Si_3N_4 on SiO_2 with even more volatile organic solvents as isopropanol, cyclohexane and hexane that lasted for more than 96 hours [39]. These long lifetimes were attributed to capillary and wetting forces that resist evaporation, but a more detailed explanation was not given. Our observations of a rapid evaporation of a rather non-volatile liquid in ~200 nm diameter holes are consistent with estimates of the evaporation rates, as derived in this section. The observation of the stability of liquids with many orders of magnitude higher vapor pressures in similar or larger geometries indicates that there are still unidentified effects that may play a role.

6. Conclusion

We created a double heterostructure cavity by selectively infiltrating a silicon PhC waveguide with LC. By measuring the time evolution of the associated spectra, we investigated the LC dynamics in our system below and above the phase transition and explored its stability due to liquid transport and evaporation. We showed that evaporation occurred, even at room temperature. The optical results were analyzed by modeling the microcavity as a FP in order to account for the joint effect of the cavity length shrinkage and the reduction of the volume of liquid (~10% in 35min at 20°C). We also correlated the measured evaporation with the vapor pressure of LCs, and showed that despite its relatively low value, evaporation has a significant impact due to the small volume of liquids involved in the experiment. These conclusions are not specific to the liquid used, although some groups have reported an apparent stability of PhCs infiltrated with other liquids. This suggests that other factors may govern the evaporation rate of ultra small amounts of liquids. Beside the possibility to optimize the pattern of the infused liquid to restrict the evaporation rate, this work highlights that special care should be taken when dealing with selectively infiltrated PhC structures, and points to the potential necessity of a sealed environment.

Acknowledgements

This work was supported by an Australian Research Council (ARC) under the ARC Centres of Excellences and Linkage Programs. We also acknowledge L. O'Faolain and T. Krauss, St. Andrews University for the fabrication of the PhCs. ST-H is supported by the ARC Australian Research Fellowship (DP1096288).